
# Intrinsic polarization-sensitive organic photodetector with self-assembled all-polymer heterojunction

Applied Physics Letters ARTICLE scitation.org/journal/apl

# Intrinsic polarization-sensitive organic photodetector with self-assembled all-polymer heterojunction

Cite as: Appl. Phys. Lett. **121**, 233301 (2022); doi: 10.1063/5.0128850
Submitted: 30 September 2022 · Accepted: 21 November 2022 ·
Published Online: 6 December 2022



Xuhao Luo,[1] Yingying Xue,[1] Juntao Wu,[1] Wanzhu Cai,[1,a)] Daniela Täuber,[2,a)] Ivan Malovicho,[3] Bogdan Sava,[3] Guobiao Cen,[1] Xing Lu,[1] Chuanxi Zhao,[1] Ivan G. Scheblykin,[4] Jianhui Yu,[5] Wenjie Mai,[1] Feng Liu,[6] Ergang Wang,[7] and Lintao Hou[1,a)]

## AFFILIATIONS

[1]Guangzhou Key Laboratory of Vacuum Coating Technologies and New Energy Materials, Guangdong Provincial Engineering Technology Research Center of Vacuum Coating Technologies and New Energy Materials, Siyuan Laboratory, Department of Physics, Jinan University, Guangzhou 510632, People's Republic of China

[2]Heintzmann Lab, Leibniz Institute of Photonic Technology, Jena 07745, Germany and Institute of Physical Chemistry, Friedrich-Schiller University Jena, Jena 07743, Germany

[3]Attocube Systems AG, Haar 85540, Germany

[4]Department of Chemical Physics and NanoLund, Lund University, Lund SE-22100, Sweden

[5]Department of Optoelectronic Engineering, Jinan University, Guangzhou 510632, People's Republic of China

[6]Frontiers Science Center for Transformative Molecules, In-situ Center for Physical Science, and Center of Hydrogen Science, School of Chemistry and Chemical Engineering, Shanghai Jiao Tong University, Shanghai 200240, People's Republic of China

[7]Department of Chemistry and Chemical Engineering, Chalmers University of Technology, Göteborg SE-412 96, Sweden

[a)]**Authors to whom correspondence should be addressed:** wzhcai@jnu.edu.cn; daniela.taeuber@uni-jena.de; and thlt@jnu.edu.cn

## ABSTRACT

Intrinsic polarization-sensitive photodetectors (IPPDs) have attracted considerable attention in recent years due to their simplicity in configuration, making them ideal candidates for compact and integrated polarization-sensitive sensing and imaging systems. Photoactive films with intrinsic optical anisotropy are necessary for IPPDs. This study reports an achievement of photoactive films based on all-polymer heterojunction films with in-plane optical anisotropy using a simple bottom-up self-assembly method. Both the donor (TQ1) and acceptor (N2200) polymers have the same spatial orientation with distinct anisotropy, approaching a dichroic ratio (DR) of 8. Polarization-sensitive light absorption is due to the uniaxially oriented polymer chains, which are dominated by lamellar packing with edge-on orientation. For IPPDs based on this anisotropic all-polymer heterojunction film, a photocurrent anisotropy was found with a polarized photocurrent ratio of 2.6. The detectivity of these IPPDs was found to be $1.9 \times 10^{11}$ Jones (@ ~600 nm, 0 V bias). Our work shows that oriented polymer donor–acceptor films fabricated using bottom-up self-assembly have great potential in applications, such as polarization detection.



The donor/acceptor heterojunction is a core element of the low-cost organic optoelectronic devices, which plays an essential role in exciton dissociation and charge transport.[1–3] Heterojunctions based on organic semiconductors are generally fabricated using solution-processable techniques, such as spin-coating, which are generally distributed randomly and optically isotropic. Recently, optically anisotropic films containing well-oriented heterojunctions have been developed for organic photodetectors (OPDs) to realize detection of linearly polarized light and have received considerable attention.[4–7]

The conventional polarization-sensitive photodetector requires additional optical components, such as a polarizer, a grating, or a surface plasmon configuration,[8–10] making it challenging to meet the requirements of miniaturization and integration for optical and photonic systems.[11,12] Intrinsic polarization-sensitive photodetectors (IPPDs) based on optically anisotropic films can achieve the detection of light polarization without additional optical components. Therefore, they can potentially overcome the above-mentioned challenges.[13,14] The latest progress on organic IPPDs has been made by the groups of

O'Connor and of Hernandez-Sosa. O'Connor's group used strain alignment techniques to fabricate an all-polymer-based bulk heterojunction (BHJ) that has a dichroic ratio (DR) of up to 17, indicating that organic IPPDs have a great deal of potential for future development.[4,6] Recently, the Hernandez-Sosa group has also developed a modified air-assisted blade coating method to fabricate an orientated P3HT:N2200 film with a maximum polarization ratio of 3.5 in IPPD.[15] Table S1 summarizes some organic IPPD performance reported to date. IPPDs based on organic semiconductors inherit many advantages of organic photodetectors, such as high absorption coefficient, tuning spectral selectivity, simple processing, mechanical flexibility, and translucency.[16–19]

Strategies to realize the oriented heterojunctions are like those of oriented single polymers, which include top-down and bottom-up fabrication approaches.[19] The top-down method, such as the rubbing technique[20] and stretching alignment,[21] requires an external force to regulate the backbones of solid-state polymers. In most cases, the top-down method can cause external traumas with the limited orderliness of polymer chains, which is harmful to the performance and stability of IPPDs. In contrast, the bottom-up method induced by self-assembly driving forces at the molecular level, such as van der Waals force, can promote the assembly of polymer chains with higher orderness, better uniformity, more compact arrangement, and fewer defects. However, to date, the bottom-up self-assembly method has not yet been adapted for the fabrication of organic IPPDs, in which the orientation of the bulk heterojunction blend is spontaneously formed.

In this work, we present anisotropic all-polymer heterojunction (AAPH) films fabricated via a bottom-up self-assembly approach of the floating film transfer method (FFTM). We find that both the donor and acceptor polymers are highly oriented into a monodomain ordered structure, respectively, throughout the film. Polymer chains are dominated by the lamellar packing with a tendency towards the edge-on orientation caused by the preferential orientation of the alkyl side chains normal to the orthogonal liquid surface during self-assembly. It turns out that its DR approaches 8. Based on this film, we also developed an IPPD with an ultrathin electron transport layer (ETL) of $TiO_2$ from atomic layer deposition (ALD) to eliminate the leakage current. The photocurrent anisotropy is 2.6, and a relative detectivity (D*) up to $1.9 \times 10^{11}$ Jones (@ ~600 nm, 0 V bias). Our work demonstrates an effective approach for orientating all-polymer bulk heterojunctions and shows that IPPDs can be obtained by engineering both the molecular orientation and the interface structure.

In our work, the polymer materials used to construct the heterojunction are poly[2,3-bis(3-octyloxyphenyl)-quinoxaline-5,8-*diyl*-alt-thiophene-2,5-diyl] (TQ1)[22] as donor and poly[1,8-bis(dicarboximide)-2,6-*diyl*]-alt-5,5′-(2,2′-bithiophene) (N2200) [Fig. 1(a)][23] as acceptor. In a previous study of a self-assembled orientated TQ1 film, we showed that the chains of the TQ1 conjugated polymers exhibit highly ordered conformation and the transition dipole moments are perfectly aligned,[24] resulting in excellent polarized absorption and emission characteristics.[14] In this study, N2200 is introduced into the film with TQ1 to create all-polymer heterojunctions (Fig. S1).

The AAPH film of TQ1:N2200 was fabricated by FFTM[14,25,26] and transferred to the top of ETL [Fig. 1(b)]. Isotropic all-polymer heterojunction (IAPH) fabricated from spin-coating is the reference. The AAPH film has a typical strip-like shape with a thickness of ~30 nm (Fig. S2).[14] The strip spreads during the self-assembly process until the volume of the injected solution is spread. More details of the fabrication process can be found in the supplementary material. First, the images of the obtained film were checked using the polarized light microscope (PLM) under cross-polarized illumination [Fig. 1(c)]. By rotating the film mounted to the microscope stage with angular steps of 45°, a variation between maximum and minimum brightness is observed. This indicates that both TQ1 and N2200 molecules have the same spatial orientation with distinct anisotropy. The whole AAPH

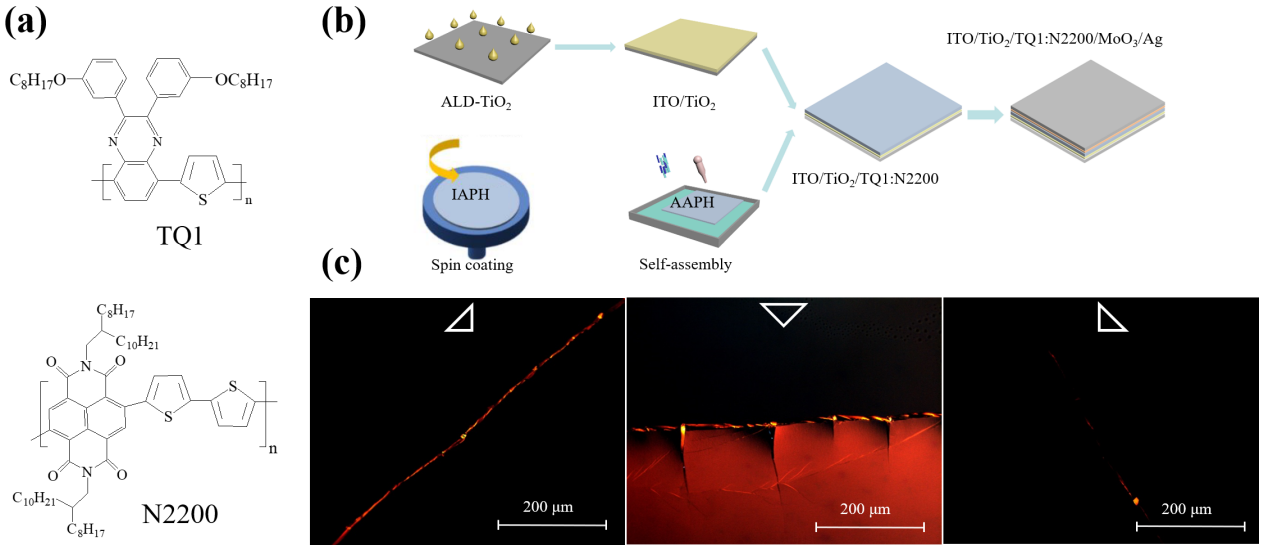


**FIG. 1.** (a) The chemical structures of TQ1 and N2200 polymers. (b) The schematic diagram of the whole fabrication processes of conventional and polarization-sensitive OPDs. (c) Microscopy images of the AAPH film under cross-polarized detection at -45° (left), 0° (middle), and 45° (right) in respect to the linearly polarized illumination. The triangle symbol represents a reference mark of rotation of the AAPH film (scale bar is 200 $\mu$m).

film is optically uniform (the cracked edge of the film was specifically selected as a reference). Furthermore, to probe the alignment direction of the backbone of conjugated polymers, the pristine TQ1 and N2200 films fabricated using the same procedure were investigated using two-dimensional polarization imaging (2D POLIM) (Fig. S3), which provides the orientation angle ($\theta_{em}$) and the modulation depth of polarization ($M_{em}$) (defined in the supplementary material). In a previous study, millimeter-sized homogeneously aligned areas were found from a pristine TQ1 film fabricated by FFTM. In these areas, the polymer chains were found to align perpendicularly to the spreading direction of the film.[14] The pristine TQ1 and N2200 polymers show similar $\theta_{em}$ about 60°–110° which is roughly perpendicular to the spreading directions of these films. Hereafter, the direction perpendicular to the spreading direction is also referred to the polymer chain orientation direction. The $M_{em} \approx 0.4$ for the pristine N2200 film is slightly lower than $M_{em} \approx 0.5$ for the pristine TQ1 film. The slightly less order of N2200 chains may be due to the big fused-ring structure of naphthalene diimide in comparison to the more linear structure of TQ1.

The anisotropic optical characteristics of the AAPH film were further studied using polarized UV–Vis spectroscopy and compared to the conventional IAPH film processed by spin-coating. In the case that the orientation of linearly polarized illumination is parallel to the polymer chain orientation (//) for the AAPH film, the absorption intensity reaches a maximum value over a wide spectral range from 350 to 900 nm, whereas the absorption intensity reaches a minimum value when the linearly polarized illumination is perpendicular to the polymer chain orientation (⊥) [Fig. 2(a)]. In contrast, anisotropic optical absorption was not found in the IAPH film with negligible dependence of absorption intensity on orthogonal light polarization [Fig. 2(c)]. Furthermore, the absorption intensities at the characteristic wavelengths of 640 and 800 nm show an ideal $\cos^2(\theta)$ dependence (Malus's law) on the light polarization angle ($\theta$) [Fig. 2(b), polar plot for 640 nm shown in Fig. S4], whereas there is no intensity modulation with varied $\theta$ for the IAPH film [Fig. 2(d)]. The above-mentioned results indicate that there is a spatial alignment of both TQ1 and N2200 polymer chains in the AAPH film processed by the bottom-up self-assembly method, while the conventional donor–acceptor film processed by spin-coating is isotropic. In addition, there is a redshift of about 10 nm in the absorption spectrum of the self-assembly AAPH film compared to the spin-coated IAPH film (Fig. S5), which points to better polymer self-organization and a longer $\pi$-conjugation length in the AAPH film.[27,28] Actually, the films of pristine TQ1 and N2200 processed by the bottom-up self-assembly method also exhibit an anisotropic light absorption feature [Figs. S6(a) and S6(b)] with the same spatial orientation perpendicular to the film propagation direction (Fig. S2), which is consistent with their fluorescence emissions (Fig. S3).

The AAPH film exhibits DR > 7.5 at two apparent characteristic peaks of 480 and 770 nm, and DR ≥ 4 in the whole spectral region (Fig. S7). Further information is obtained from evaluating the degree of order of the arrangement of polymer chains, denoted $\mathcal{O}$, which is defined as $\mathcal{O} = \frac{DR-1}{DR+2}$.[29] A value of $\mathcal{O} = 0.5$ at the absorption peak at 640 nm indicates that the AAPH tends to be a uniaxially oriented all-polymer blend rather than a randomly distributed mixture. The pristine TQ1 and N2200 films yield $\mathcal{O} = 0.48$ and $\mathcal{O} = 0.46$, respectively, demonstrating an improved molecular alignment for the polymer blend. The above-mentioned findings confirm that the alignment of polymer chains in the AAPH film induces an optical anisotropy.

The AFM topography of the AAPH film reveals a stripe-type lamellar structure in both height and high-precision phase mode images, whereas a random pattern is seen in the AFM images of the

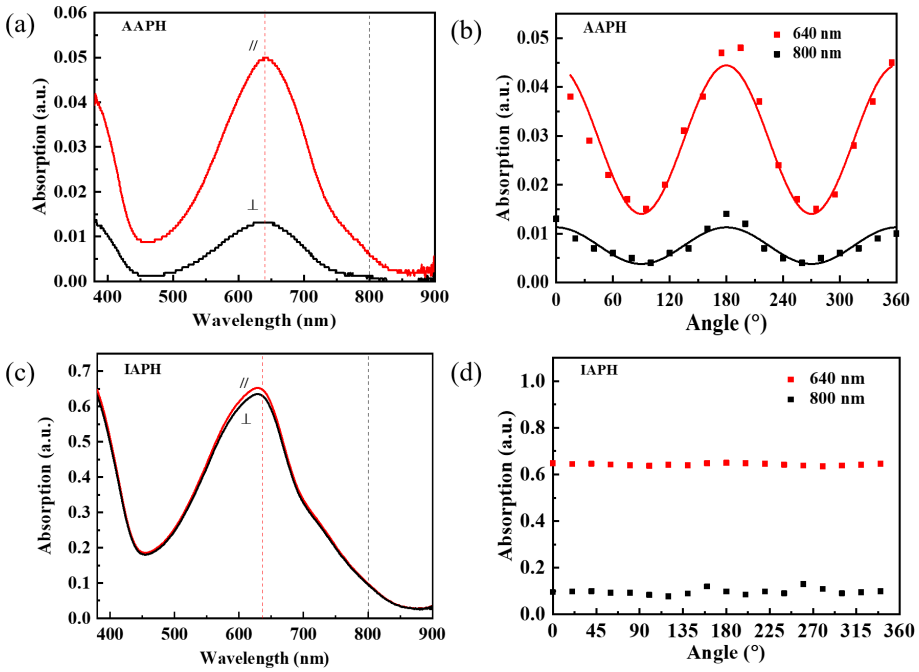


FIG. 2. Polarized UV–Vis absorption spectra of the (a) AAPH and (c) IAPH films. Symbols of // and ⊥ correspond to the polymer chain orientation parallel and perpendicular to the polarization direction of the incident light. The dependence of the absorption intensity on the $\theta$ for the (b) AAPH and (d) IAPH films at 640 and 800 nm with the fitting lines based on Malus's law.

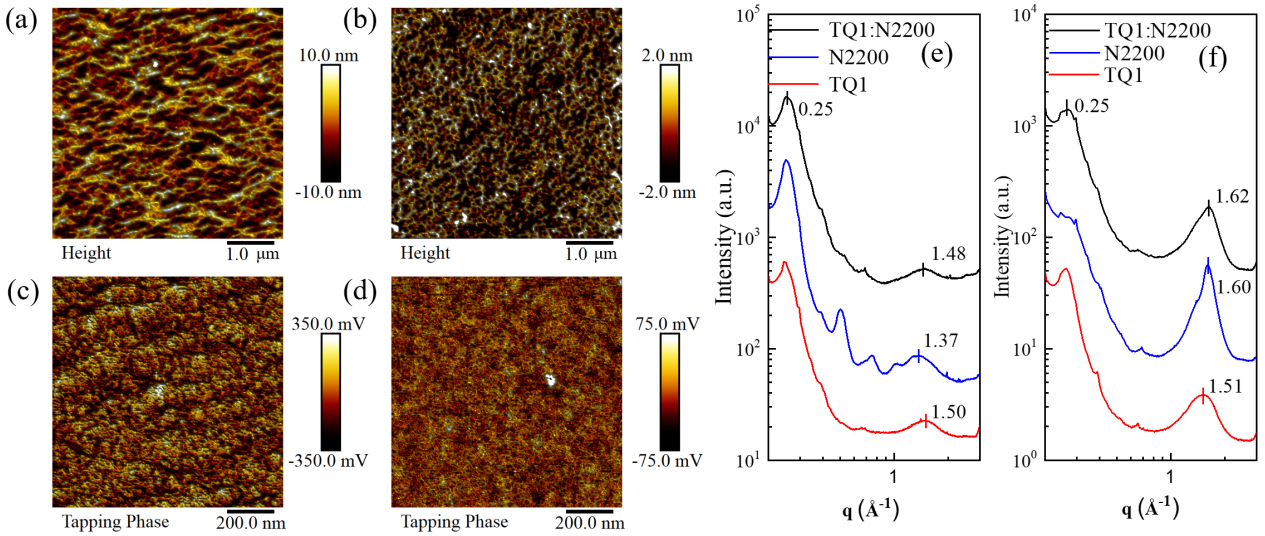


**FIG. 3.** AFM height and phase images of the (a) and (c) AAPH and (b) and (d) IAPH TQ1:N2200 films. GIXD out-of-plane profiles of the (e) AAPH, N2200, and TQ1 films by the bottom-up self-assembly method, compared to those of the (f) IAPH, N2200, and TQ1 films by spin-coating.

IAPH film [Figs. 3(a)–3(d)]. GIXD complements the information on the local nanostructure by revealing the long-range order structure. The out-of-plane profiles of both polymer blend films and pristine TQ1 and N2200 films by the bottom-up self-assembly method and spin-coating are presented in Figs. 3(e) and 3(f) (Fig. S8), respectively. A distinct (100) peak at 0.25 $Å^{-1}$, corresponding to a lamellar packing distance of around 24.2 Å,[30–32] appears in the out-of-plane profile of the TQ1:N2200 AAPH film, which approximately matches the (100) peak position obtained from the pristine TQ1 and N2200 films fabricated by the bottom-up self-assembly method [Fig. 3(e)]. However, the (100) peak at 0.25 $Å^{-1}$ seen in the out-of-plane profiles of the IAPH film and the spin-coated pristine TQ1 film are much broader [Fig. 3(f)], and this peak almost disappeared in the spin-coated pristine N2200 film, not to mention the (200) peak centered at 0.5 $Å^{-1}$ for the pristine N2200 film fabricated by the bottom-up self-assembly method [Fig. 3(e)]. Additionally, the (010) diffraction peak at 1.51–1.60 $Å^{-1}$, which corresponds to the $\pi$–$\pi$ stacking of polymer backbones, appears broader and shifted to smaller q at 1.37–1.50 $Å^{-1}$ with decreased intensity in the AAPH, pristine N2200 and TQ1 films fabricated by the bottom-up self-assembly compared to the corresponding films fabricated by spin-coating. It suggests that the intermolecular $\pi$–$\pi$ packing in the AAPH film is a bit looser than that in the IAPH film and the organization of polymer backbones in the AAPH film is dominated by the lamellar packing with a tendency towards the edge-on orientation caused by the preferential orientation of the alkyl side chains normal to the orthogonal liquid surface during self-assembly. Thus, the optical orientation can be explained by the highly ordered polymer chain alignment structure.

In addition to the structural evaluation using conventional AFM and GIXD, direct access to nanoscale chemical characterization of the AAPH film is further provided by a recently developed nano-infrared spectroscopy method combining powerful mid IR excitation and mechanical probing via AFM.[33] In tapping AFM-IR, an incident pulsed IR beam induces a thermal expansion of the sample,[34] which modulates the interaction force with the metallic AFM probe. A micrometer-sized region of the AAPH film was investigated at three mid IR frequencies of 1664, 1401, and 1340 $cm^{-1}$ in succeeding scans [Figs. 4(a)–4(c)] with displaying the corresponding AFM height images in Figs. 4(d)–4(f), respectively. Figure S9(a) shows that the incident mid-IR light from the quantum cascade laser illuminates the sample with a large incidence angle, ~70°, and it is linearly polarized in the plane of incidence. Consequently, under this condition, vibrations oriented out-of-plane in respect to the sample surface are preferentially excited. Tapping AFM-IR image displays the qualitative spatial orientation of the corresponding chemical bonds in the sample. It has been reported that the strong band at 1664 $cm^{-1}$ in the FTIR spectrum of pristine N2200 corresponds to the in-plane anti-symmetric C=O stretching vibration of the naphthalene-dicarboximide (NDI) moiety which is parallel to the N2200 polymer backbone.[35–37] The strong tapping AFM-IR signal at 1664 $cm^{-1}$ in Figs. 4(a) and 4(g) illustrates an out-of-plane tilt orientation of N2200 in the AAPH film. The slight drop in signal intensity seen in the lower right region of Fig. 4(a) might point to an orientation of the NDI moiety parallel to the film surface. On the other hand, the tapping AFM-IR signal intensity obtained at 1340 $cm^{-1}$ is very uniform and high except for the depression line also seen in the height images [Figs. 4(c) and 4(f)]. In the FTIR spectrum of TQ1, a band appears at 1340 $cm^{-1}$, which is related to the C–O stretching vibration of the phenyl moieties [Fig. 4(g)]. The result might indicate an out-of-plane sloping orientation of TQ1; however, this has to be further confirmed by spatially resolved studies of vibrational transitions in TQ1. The tapping AFM-IR signal intensity at 1401 $cm^{-1}$ is relatively high in the whole region except for some stronger sporadic microarea [Fig. 4(b)], revealing that most of N2200 chains are oriented in the direction tilting toward out-of-plane to the AAPH film surface. Figure S9b illustrates the orientation of the corresponding vibrational transition moment in N2200. The derived change in the in-plane orientation and the out-of-plane tilt orientation of the molecular structure is depicted in the AFM

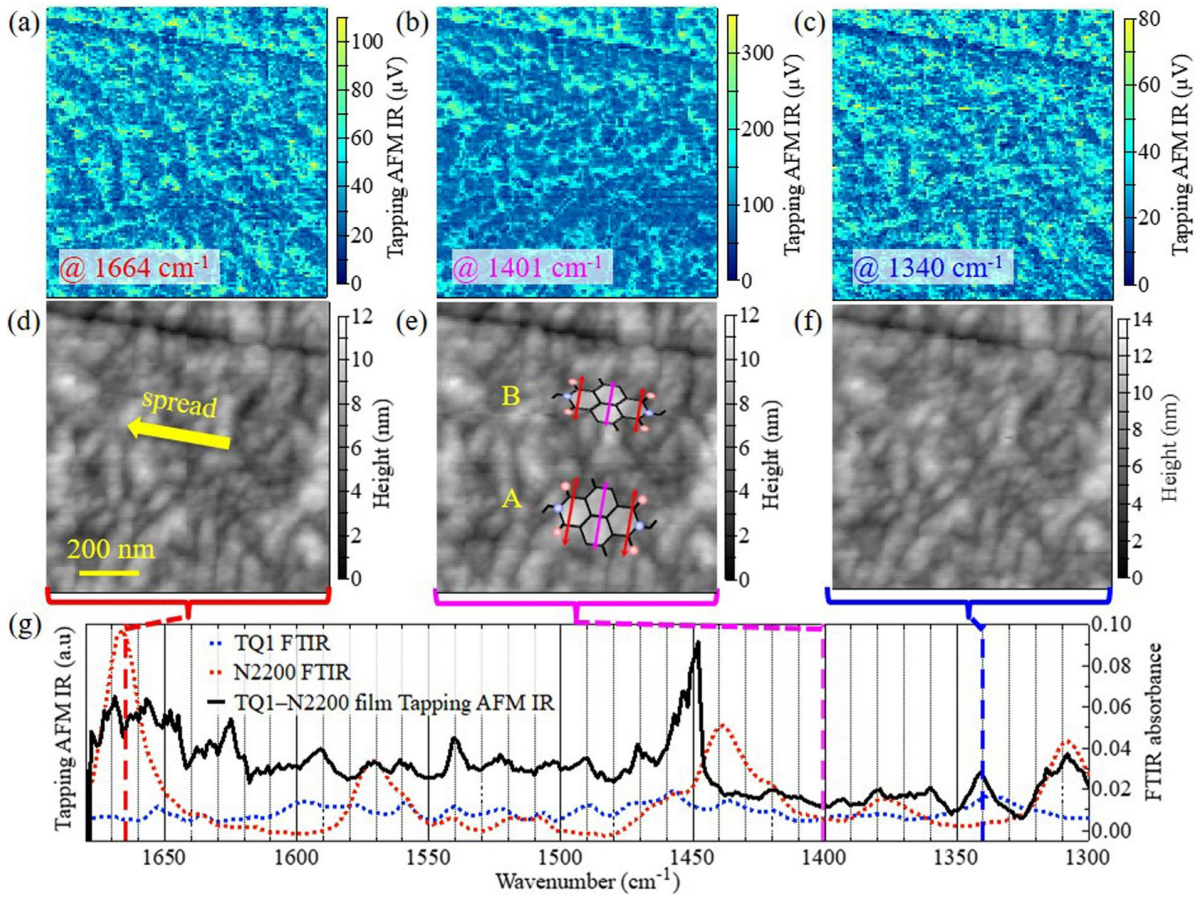


**FIG. 4.** Tapping AFM-IR intensity of the AAPH film recorded during succeeding scans of the same film region at mid-IR excitation frequency of (a) 1664, (b) 1401, and (c) 1340 $cm^{-1}$, respectively. (d–f) Simultaneously obtained corresponding AFM height images with the indicated direction of the AAPH film spreading. Schematics present the derived in-plane and out-of-plane orientation of the NDI ring structure in area A and B, respectively, whereby arrows depict the orientation of important vibrational transitions. (g) Tapping AFM-IR spectrum of the AAPH film in comparison with FTIR spectra of pristine TQ1 and pristine N2200 bulk materials. The color dashed lines mark the frequencies of the three individual scans.

height image [Fig. 4(e)]. The results are in accordance with the macroscopically measured degree of molecular order as well as with the GIXD measurements. Further studies on flow characteristics and the design of suitable devices aiming at the improved in-plane orientation of the polymer chains by the bottom-up self-assembly method will bear the potential of reaching even higher sensitivity for polarization in such films.

Based on an AAPH film, we initially fabricated a device with a diode structure of ITO/PFN/AAPH/$MoO_3$/Ag, in which PFN is a widely used interfacial layer of poly[(9,9-bis(3′-(N,N-dimethylamino)-propyl)-2,7-fluorene)-alt-2,7–(9,9-dioctyfluorene)] (Fig. S10). However, the device presented a low rectification ratio of 10 at ±1 V in the dark. When PFN was replaced by the $TiO_2$ fabricated from ALD, the corresponding device showed a good rectification ratio of $10^3$ at ± 1V, mainly due to the reduced dark current under reverse voltage. It suggests the modified device structure presented a better rectifying behavior of carriers. More importantly, the suppressed dark current resulted in a low shot noise, which played an important role among the many sources of noise in OPD. Figure 5(a) shows the current density−voltage ($J-V$) characteristics of the optimized device measured in the dark and under 660 nm laser irradiation at 3.35 and 17.21 $mW/cm^2$. Figure 5(b) shows the relationship between the photocurrent and the polarization angle for the corresponding OPD with a reference device of an IAPH based OPD. Similar with the profiles of absorption−angle curves (Fig. 2), the photocurrent of the IPPD changes in a period of 180° with a maximum photocurrent value 2.6 times higher than the minimum one, while the photocurrent of the IAPH-based OPD remains almost constant with respect to the variation of polarization angles.

Figure 5(c) shows the spectral responsivity (R) from 350 to 750 nm under bias of 0 and −0.5 V. The peak responsivity of 0.034 A/W is obtained at the wavelength of 610 nm under zero bias, which is consistent with the maximum absorption peak of the AAPH film. When the bias increases to −0.5 V, the corresponding spectral responsivity increases to 0.050 A/W, because the reverse bias can increase the photocurrent collection. Then, we measured the total noise current ($i_n$) of the devices from 1 to $10^5$ Hz under different bias.

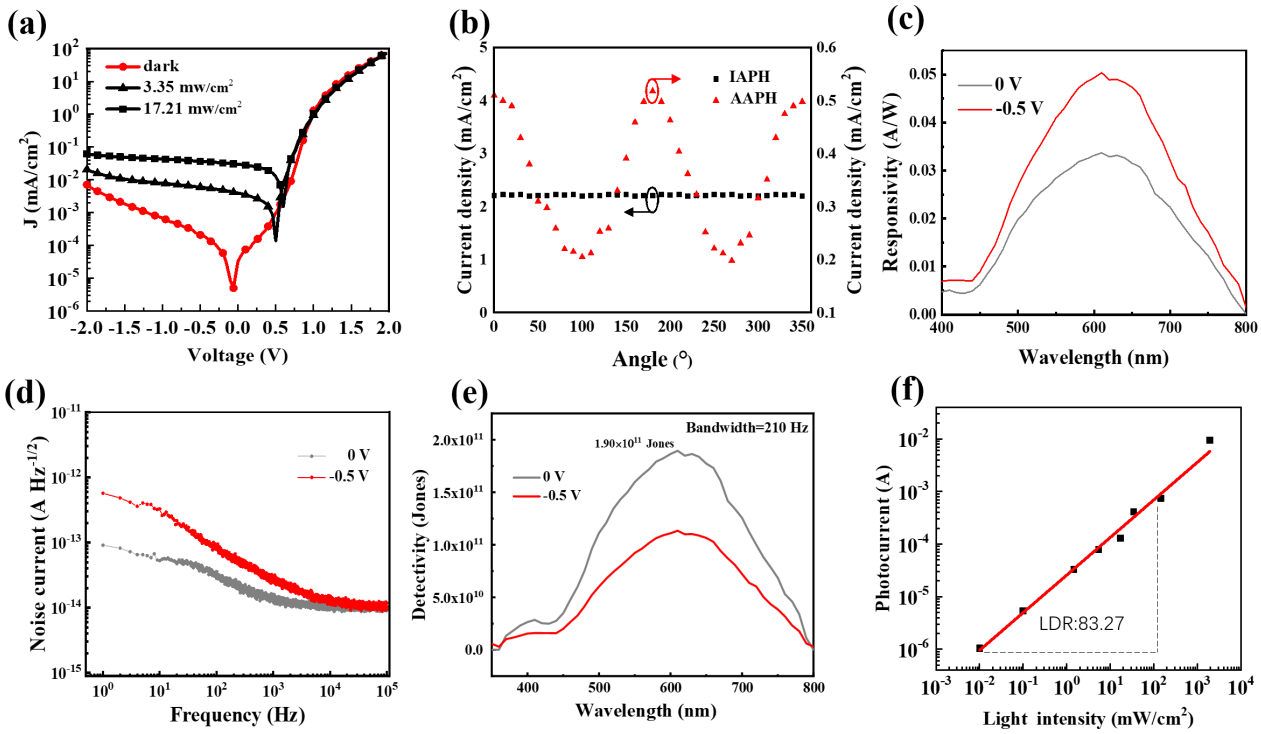


**FIG. 5.** (a) $J-V$ curves of the AAPH-based OPD in the dark and under the illumination of 3.35 and 17.21 mW/cm$^2$ (@660 nm), (b) The dependence of the photocurrent on the variation of $\theta$ under white-light illumination of 100 mW/cm$^2$ for the IAPH and AAPH-based OPDs. (c) The spectral responsivity, (d) noise current, and (e) specific detectivity of the AAPH-based OPD under 0 and -0.5 V bias. (f) The linear dynamic range of the AAPH-based photodetector under 600 nm laser illumination.

As displayed in Fig. 5(d), $i_n$ is bias-dependent and frequency-dependent. 1/f noise dominates the noise current in the low frequency range. In the high frequency range, the total noise current of the photodetector approaches its shot noise limit. Under 0 and $-0.5$ V bias, the noise current is saturated at a smaller frequency, which is frequency-independent. The noise density at a bias of 0 and $-0.5$ V were $2.23 \times 10^{-14}$ and $5.58 \times 10^{-14}$ A Hz$^{-1/2}$ at a modulation frequency of 210 Hz, respectively [Fig. 5(e)].[38,39] We find that the detectivity is maximized at the $-0.5$ V, which is above $1.9 \times 10^{11}$ Jones at about 600 nm. This decent detectivity is attributed to the optimized device configuration with $TiO_2$ fabricated from ALD as ETL, which resulted in a reduced dark current under reverse voltage. It suggests the modified device structure presented a better rectifying behavior of carriers. More importantly, the suppressed dark current resulted in a low shot noise, which played an important role among the many sources of noise in OPD.

Figure 5(f) shows the dependence of the photocurrent (I) on the illumination power density ($P$) at $\lambda = 660$ nm. A power-law relationship of $I \propto P^{0.715}$ is extracted by the fitting. The fitting factor of $0.715 < 1.0$ implies that geminate or nongeminate charge recombination exists in the IPPD. Furthermore, in the linear dynamic range (LDR), the AAPH-based OPD presents a wide LDR of 83 dB.

This paper presents a simple bottom-up self-assembly method to achieve a photoactive film based on all-polymer heterojunction films with in-plane optical anisotropy. The optical anisotropy results from the uniaxially oriented polymer chains, which are dominated by lamellar packing with edge-on orientation. It has been found that IPPDs based on these AAPH films exhibit polarized photocurrent anisotropy with a ratio of 2.6 with a detectivity of $1.9 \times 10^{11}$ Jones. This self-assembly method shows some clear advantages over the top-down orientation method in terms of AAPH films with high order, uniformity, compact arrangement, and few defects.

See the supplementary material for information regarding parameter introduction, performance summary for organic IPPDs, the energy levels of TQ1 and N2200, schematic diagram of the formation process of the AAPH film, polarization angle and modulation depth, polar plot of angular dependence of absorption, normalized absorption spectra of the spin-coated and self-assembled TQ1:N2200 films, anisotropic optical absorption characteristics of the pristine TQ1 and N2200, the dichroic ratio spectrum of the AAPH film, GIXD images, schematic illustration of the geometry used in tapping AFM-IR, and the J–V curves of the devices in the dark.

The authors thank Jieyuan Tang (JNU-DOE, Guangzhou) for the help on polarized light microscope testing and Christoph Krafft (Leibniz-IPHT, Jena) for help with FTIR measurements. The authors gratefully acknowledge funding from the National Natural Science Foundation Project (Nos. 61774077, 61804065, 51973100, and 21734009), High-End Foreign Experts Project (Nos. 2020A1414010036 and G20200019046), the Key Projects of Joint Fund of Basic and Applied Basic Research Fund of Guangdong

Province (No. 2019B1515120073), the Guangdong Basic and Applied Basic Research Foundation (No. 2021A1515012561), and the Science and Technology Planning Project of Guangzhou (Nos. 201804010295 and 201605030008). D.T. acknowledges funding by the German Research Foundation (Nos. 256530768 and 439139881). A portion of this work was performed on beamlines 7.3.3 and 11.0.1.2 at the Advanced Light Source, Lawrence Berkeley National Laboratory, supported by the DOE, Office of Science, and Office of Basic Energy Sciences.

## AUTHOR DECLARATIONS

### Conflict of interest

The authors have no conflicts to disclose.

### Author Contributions

**Xuhao Luo:** Data curation (lead). **Chuanxi Zhao:** Methodology (supporting); Resources (supporting). **Ivan Scheblykin:** Methodology (equal). **Jianhui Yu:** Resources (supporting). **Wenjie Mai:** Methodology (supporting); Resources (supporting). **Feng Liu:** Data curation (equal); Methodology (equal). **Ergang Wang:** Methodology (supporting). **Hou Lintao:** Supervision (equal); Writing – original draft (supporting); Writing – review & editing (equal). **Yingying Xue:** Data curation (equal); Formal analysis (equal). **Juntao Wu:** Data curation (supporting); Formal analysis (supporting). **Wanzhu Cai:** Conceptualization (lead); Supervision (lead); Writing – original draft (lead); Writing – review & editing (lead). **Daniela Täuber:** Data curation (equal); Investigation (equal); Methodology (equal); Supervision (supporting); Writing – review & editing (equal). **Ivan Malovicho:** Data curation (supporting); Resources (supporting); Software (supporting). **Bogdan Sava:** Data curation (supporting); Resources (supporting); Software (supporting). **Guobiao Cen:** Methodology (supporting). **Xing Lu:** Resources (supporting).

## DATA AVAILABILITY

The data that support the findings of this study are available from the corresponding author upon reasonable request.

## REFERENCES

[1]Q. Liu, Y. Jiang, K. Jin, J. Qin, J. Xu, W. Li, J. Xiong, J. Liu, Z. Xiao, and K. Sun, "18% efficiency organic solar cells," Sci. Bull. **65**, 272–275 (2020).
[2]Z. Zhao, M. Liu, K. Yang, C. Xu, Y. Guan, X. Ma, J. Wang, and F. Zhang, "Highly sensitive narrowband photomultiplication-type organic photodetectors prepared by transfer-printed technology," Adv. Funct. Mater. **31**, 2106009 (2021).
[3]Z. Lan, Y. S. Lau, Y. Wang, Z. Xiao, L. Ding, D. Luo, and F. Zhu, "Filter-free band-selective organic photodetectors," Adv. Opt. Mater. **8**, 2001388 (2020).
[4]P. Sen, R. Yang, J. J. Rech, Y. Feng, C. H. Y. Ho, J. Huang, F. So, R. J. Kline, W. You, M. W. Kuddenov, and B. T. O'Connor, "Panchromatic all-polymer photodetector with tunable polarization sensitivity," Adv. Opt. Mater. **7**, 1801346 (2019).
[5]A. Altaqui, P. Sen, H. Schrickx, J. Rech, J. W. Lee, M. Escuti, W. You, B. Kim, R. Kolbas, B. T. O'connor, and M. Kudenov, "Mantis shrimp-inspired organic photodetector for simultaneous hyperspectral and polarimetric imaging," Sci. Adv. **7**, eabe3196 (2021).
[6]H. M. Schrickx, P. Sen, R. E. Booth, A. Altaqui, J. Burleson, J. J. Rech, J.-W. Lee, M. Biliroglu, K. Gundogdu, B. J. Kim, W. You, M. W. Kudenov, and B. T. O'Connor, "Ultra-high alignment of polymer semiconductor blends enabling photodetectors with exceptional polarization sensitivity," Adv. Funct. Mater. **32**, 2105820 (2022).
[7]A. Altaqui, H. Schrickx, P. Sen, L. Li, J. Rech, J. W. Lee, N. Balar, W. You, B. J. Kim, M. Escuti, R. Kolbas, B. T. O'Connor, and M. Kudenov, "Bio-inspired spectropolarimetric sensor based on tandem organic photodetectors and multi-twist liquid crystals," Opt. Express **29**, 43953–43969 (2021).
[8]D. Wu, J. Guo, J. Du, C. Xia, L. Zeng, Y. Tian, Z. Shi, Y. Tian, X. J. Li, Y. H. Tsang, and J. Jie, "Highly polarization-sensitive, broadband, self-powered photodetector based on graphene/$PdSe_2$/germanium heterojunction," ACS Nano **13**, 9907–9917 (2019).
[9]R. M. Matchko and G. R. Gerhart, "High-speed imaging chopper polarimetry," Opt. Eng. **47**, 016001 (2008).
[10]Y. Zhao and A. Alù, "Manipulating light polarization with ultrathin plasmonic metasurfaces," Phys. Rev. B **84**, 205428 (2011).
[11]R. M. A. Azzam, "Arrangement of Four photodetectors for measuring the state of polarization of light," Opt. Lett. **10**, 309–311 (1985).
[12]J. J. Foster, S. E. Temple, M. J. How, I. M. Daly, C. R. Sharkey, D. Wilby, and N. W. Roberts, "Polarisation vision: Overcoming challenges of working with a property of light we barely see," Sci. Nat. **105**, 27 (2018).
[13]H. Yuan, X. Liu, F. Afshinmanesh, W. Li, G. Xu, J. Sun, B. Lian, G. Ye, Y. Hikita, Z. Shen, S. Zhang, X. Chen, M. Brongersma, and Y. Cui, "Broadband linear-dichroic photodetector in a black phosphorus vertical pn junction," arXiv:1409.4729.
[14]D. Täuber, W. Cai, O. Inganas, and I. G. Scheblykin, "Macroscopic domains within an oriented TQ1 film visualized using 2D polarization imaging," ACS Omega **2**, 32–40 (2017).
[15]Y. Yao, Y. Liang, V. Shrotriya, S. Xiao, L. Yu, and Y. Yang, "Plastic near-infrared photodetectors utilizing low band gap polymer," Adv. Opt. Mater. **19**, 3979–3983 (2007).
[16]M. Wu, Z. Jiang, X. Lou, F. Zhang, D. Song, S. Ning, M. Guo, S. J. Pennycook, J. Dai, and Z. Wen, "Flexoelectric thin-film photodetectors," Nano Lett. **21**, 2946–2952 (2021).
[17]H. Ren, J. Chen, Y. Li, and J. Tang, "Recent progress in organic photodetectors and their applications," Adv. Sci. **8**, 2002418 (2021).
[18]S. Gielen, C. Kaiser, F. Verstraeten, J. Kublitski, J. Benduhn, D. Spoltore, P. Verstappen, W. Maes, P. Meredith, A. Armin, and K. Vandewal, "Intrinsic detectivity limits of organic near-infrared photodetectors," Adv. Mater. **32**, 2003818 (2020).
[19]L. Zhai, S. I. Khondaker, J. Thomas, C. Shen, and M. McInnis, "Ordered conjugated polymer nano- and microstructures: Structure control for improved performance of organic electronics," Nano Today **9**, 705–721 (2014).
[20]L. Biniek, S. Pouget, D. Djurado, E. Gonthier, K. Tremel, N. Kayunkid, E. Zaborova, N. Crespo-Monteiro, O. Boyron, N. Leclerc, S. Ludwigs, and M. Brinkmann, "High-temperature rubbing: A versatile method to align $\pi$-conjugated polymers without alignment substrate," Macromolecules **47**, 3871 (2014).
[21]P. Dyreklev, M. Berggren, O. Inganäs, M. R. Andersson, O. Wennerström, and T. Hjertberg, "Polarized electroluminescence from an oriented substituted polythiophene in a light emitting diode," Adv. Mater. **7**, 43 (1995).
[22]E. Wang, L. Hou, Z. Wang, S. Hellström, F. Zhang, O. Inganäs, and M. R. Andersson, "An easily synthesized blue polymer for high-performance polymer solar cells," Adv. Mater. **22**, 5240 (2010).
[23]H. Yan, Z. Chen, Y. Zheng, C. Newman, J. R. Quinn, F. Dötz, M. Kastler, and A. Facchetti, "A high-mobility electron-transporting polymer for printed transistors," Nature **457**, 679 (2009).
[24]V. Hernández, J. Casado, F. J. Ramírez, G. Zotti, S. Hotta, and J. T. López Navarrete, "The low frequency vibrations in clathrate hydrates," J. Chem. Phys. **104**, 9271 (1996).
[25]T. Morita, V. Singh, S. Nagamatsu, S. Oku, W. Takashima, and K. Kaneto, "Enhancement of transport characteristics in poly(3-hexylthiophene) films deposited with floating film transfer method," Appl. Phys. Express **2**, 111502 (2009).
[26]A. Dauendorffer, S. Miyajima, S. Nagamatsu, W. Takashima, S. Hayase, and K. Kaneto, "One-step deposition of self-oriented $\beta$-phase polyfluorene thin films